Electronic Supplementary Material (ESI) for Energy & Environmental Science.


# Supplementary Information

## Opportunities to improve the net energy performance of photoelectrochemical water-splitting technology

*Roger Sathre, Jeffery B. Greenblatt, Karl Walczak, Ian D. Sharp, John C. Stevens, Joel W. Ager III, Frances A. Houle*

dx.doi.org/10.1039/C5EE03040D

**Contents:**

S1. Composition and embodied energy of thin film layers

S2. Embodied energy of precursor and final materials

S3. Encapsulation materials properties and selection

S4. Module frame design

S5. Panel structural design

S6. Facility location and solar insolation

S7. Monte Carlo simulation of balance-of-system energy use

S8. Module heating to avoid freezing

S9. Hydrogen demand scale-up scenarios

S10. Additional references used in the Supplemental Information

## S1. Composition and embodied energy of thin film layers

**Table S1.** Assumed properties and compositions of thin film layers, and resulting specific embodied energy of the elements comprising the layers. A material utilization efficiency ($F_m$) of 50% is assumed when calculating the specific embodied energy, i.e. half the material is wasted so twice the amount of material in the final film must be sourced. The total specific embodied energy for each film material is summarized in Figure S1.

| Film material | Material density | Film thickness | Element | Percent by weight | Embodied energy (per kg) | Embodied energy (per m$^2$) |
|---|---|---|---|---|---|---|
| | kg/m$^3$ | nm | | % | MJ/kg | MJ/m$^2$ |
| *Photoelectrode layers* | | | | | | |
| InP | 4810 | 250 | | 100% | | 5.0 |
| | | | In | 79% | 2570 | 4.9 |
| | | | P | 21% | 230 | 0.12 |
| InGaP | 4474 | 250 | | 100% | | 4.7 |
| | | | In | 47% | 2570 | 2.7 |
| | | | Ga | 28% | 3030 | 1.9 |
| | | | P | 25% | 230 | 0.13 |
| GaAs | 5320 | 250 | | 100% | | 4.1 |
| | | | Ga | 48% | 3030 | 3.9 |
| | | | As | 52% | 140 | 0.19 |
| $WO_3$ | 7160 | 250 | | 100% | | 2.3 |
| | | | W | 79% | 820 | 2.3 |
| | | | O | 21% | 0 | 0 |
| a-Si | 2330 | 250 | Si | 100% | 960 | 1.1 |
| $BiVO_4$ | 5920 | 250 | | 100% | | 2.0 |
| | | | Bi | 65% | 700 | 1.3 |
| | | | V | 16% | 1430 | 0.67 |
| | | | O | 20% | 0 | 0 |
| CdTe | 5850 | 250 | | 100% | | 0.34 |
| | | | Cd | 47% | 70 | 0.093 |
| | | | Te | 53% | 160 | 0.24 |
| $Cu_2O$ | 6000 | 250 | | 100% | | 0.092 |
| | | | Cu | 89% | 34 | 0.092 |
| | | | O | 11% | 0 | 0 |
| $Fe_2O_3$ | 5745 | 250 | | 100% | | 0.046 |
| | | | Fe | 70% | 25 | 0.046 |
| | | | O | 30% | 0 | 0 |
| *Catalyst layers* | | | | | | |
| Pt | 21450 | 1 | Pt | 100% | 263000 | 11 |
| $IrO_x$ | 22420 | 1 | Ir | 100% | 65000 | 2.9 |
| NiMo | 9594 | 1 | | 100% | | 0.0031 |
| | | | Ni | 38% | 180 | 0.0013 |
| | | | Mo | 62% | 150 | 0.0018 |
| $NiFeO_x$ | 8389 | 1 | | 100% | | 0.0019 |
| | | | Ni | 51% | 180 | 0.0017 |
| | | | Fe | 49% | 25 | 0.00019 |
| $Fe_3P$ | 6740 | 1 | | 100% | | 0.00077 |
| | | | Fe | 84% | 25 | 0.00028 |

| | | | | | | |
|---|---|---|---|---|---|---|
| | | | P | 16% | 230 | 0.00048 |
| Fe | 7870 | 1 | Fe | 100% | 25 | 0.00039 |
| *Other layers* | | | | | | |
| ITO | 7140 | 50 | | 100% | | 1.4 |
| | | | In | 74% | 2570 | 1.4 |
| | | | Sn | 8% | 320 | 0.02 |
| | | | O | 18% | 0 | 0 |
| FTO | 6950 | 50 | | 100% | | 0.17 |
| | | | F | 29% | 240 | 0.05 |
| | | | Sn | 56% | 320 | 0.13 |
| | | | O | 15% | 0 | 0 |
| $TiO_2$ | 4230 | 60 | | 100% | | 0.60 |
| | | | Ti | 60% | 1960 | 0.60 |
| | | | O | 40% | 0 | 0 |

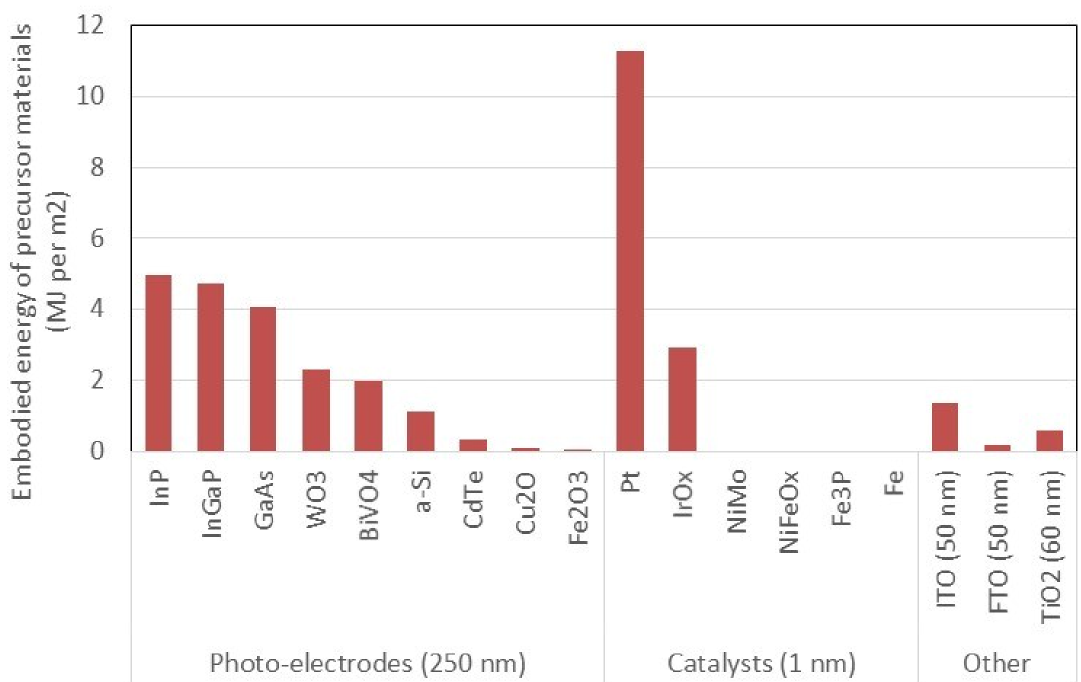


**Figure S1.** Embodied energy of precursor materials to various types of thin films, per $m^2$ of coated surface, assuming 50% product yields and 1:1 precursor material energy.

## S2. Embodied energy of precursor and final materials

Although standard life cycle inventory (LCI) databases (e.g. Ecoinvent, USLCI) contain embodied energy estimates for thousands of common commodity elements and compounds, they do not include data for tens of thousands of other specialty chemicals that are produced and used in smaller amounts. Robust quantification of the embodied energy of a diverse range of chemical compounds remains a challenge for life cycle assessment practitioners. Many of the final or precursor materials of the thin films studied here (see Section 2.2.1) are not represented in LCI databases or related literature.

There are several approaches to overcoming this knowledge gap. For example, the Finechem tool developed at ETH Zurich[S1] is a software tool to estimate the resource use and environmental impacts of the production of petrochemicals, based on their molecular structure. Ten characteristics of a chemical are entered (e.g. molecular weight, number of nitrogen atoms in the molecule, number of halogen atoms in the molecule, number of aromatic and aliphatic rings in the molecule), and the tool outputs an estimated range of cumulative energy demand for its production, as well as several other life cycle indicators.[S2] However, the range of output values is so broad that the Finechem tool provides little practical utility to LCA practitioners, and is limited to petrochemicals.

Another approach is to survey a selection of proxy materials for which LCI data are available, and use the minimum and maximum values as estimated range of the material of interest. For example, in a prospective life cycle assessment of large-scale production of metal-organic frameworks (MOFs), Sathre & Masanet[S3] estimated the range of energy use for production of MOF organic linker molecules based on proxy data on industrial-scale production of 10 benzene-based organic chemicals. The feedstock energy was found to be the dominant contributor to total energy use for all 10 materials, while the processing and supply chain energy inputs were relatively low. This suggests that the total energy intensity of other potential ligand materials would not differ significantly from this range, because they will have similar feedstock energy. They estimated the range of energy use for MOF metal supply based on data for mining and smelting of elemental metal, as well as proxy data on industrial-scale production of metal salts, e.g. from the fertilizer industry.

Due to the diversity of potential precursor materials used in thin film depositions and the paucity of life cycle inventory data on specialty chemicals, in our modeling we use a simple multiplier expressing the ratio of the embodied energy of precursor materials to the embodied energy of refined elements. In this analysis, many of the materials of interest (Figure S1 and Table S1) are relatively simple metal salt. Figure S2 shows an illustrative example of the embodied energy of two alternate production chains for a desired metallic compound used as a precursor material for thin film deposition. The metallic content of the compound begins as *in situ* ore with zero embodied energy. This ore may then be extracted and processed in various ways, with e.g. mechanical and hydraulic treatment, cumulatively increasing its embodied energy. The ore may be processed through heap leaching, where a reactive solution is repeatedly drained through a pile of ore, and a metal salt is precipitated from the solution. To produce elemental metal, the precipitate is then subject to additional energy intensive processes such as thermochemical refining. The precipitate may, however, be the desired thin film precursor material, or may be transformed into the desired material through minimal additional processing. Alternatively, after refining to elemental metal, the metal may be reacted through various processes to produce the desired metallic compound. This results in two alternate possible ranges for embodied energy of the metallic compound: a value lower than that of refined metal based on production from leachate, and a value higher than that of refined metal based on production and subsequent reaction of refined metal. LCI data are reliably available for refined elemental metals, but are not typically available for specialty metallic compounds. Therefore, and with consideration of Figure S2, we used LCI data on refined metals as our base case embodied energy for precursor materials (based on their content of elemental metal), and apply a multiplier of 2.0 for our high input case, and a multiplier of 0.5 for our low input case. This is the factor

$R_p$ described in Section 2.2.1. These quantitative values are simply assumed, as relevant data are absent in the literature. This topic is ripe for additional research by the LCA community, to develop robust estimates of the embodied energy of a diverse range of chemical feedstocks.

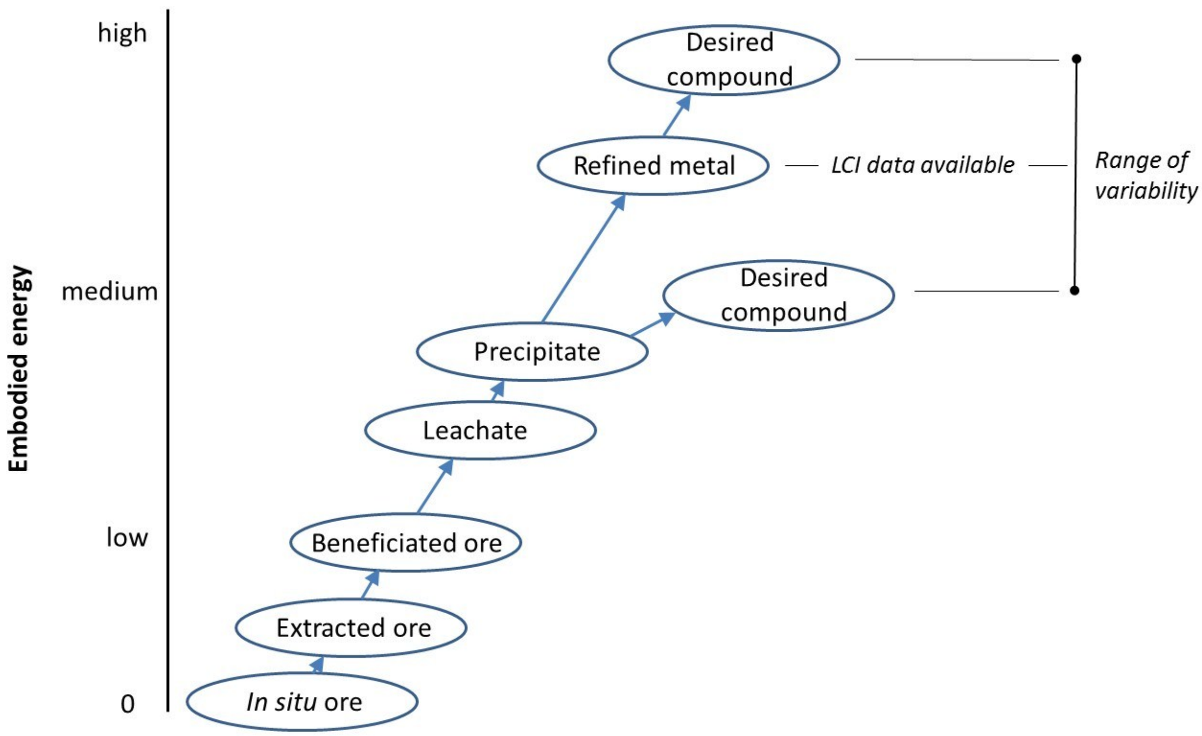


**Figure S2.** Illustrative example of the embodied energy of alternate production chains of a desired metallic compound.

## S3. Encapsulation materials properties and selection

Various materials could be used for the back cover of the PEC module. The selection of materials for the front window is more limited, although at least three light-transmissible materials are available (glass, polycarbonate and poly(methyl methacrylate)). Table S1 shows three properties (density, elastic modulus, and specific embodied energy) of six potential encapsulation materials: flat glass, rigid PVC, polycarbonate, poly(methyl methacrylate), aluminum and stainless steel. The density is lowest for the three polymer materials, highest for the stainless steel, and intermediate for the glass and aluminum. The elastic modulus (also known as Young's modulus) measures the stiffness of the materials, and is quite low for the three plastic materials. The elastic moduli of the glass and aluminum are higher and about the same, while that of stainless steel is highest. The embodied energy of a 2 mm thick sheet of each material ranges from a low of 65 MJ/m$^2$ for glass, to ~200-300 MJ/m$^2$ for the two plastic materials, to a high of >1000 MJ/m$^2$ for the two metals. Since the required thickness of a sheet is inversely proportional to its stiffness, the three plastic materials having low moduli of elasticity would need to be thicker to perform the same structural function as a 2 mm thick sheet of glass or metal. Of all six materials, glass is unique for its relatively high elastic modulus and low embodied energy. Importantly, glass also allows adequate transmissivity of light at wavelengths above 400 nm. For these reasons, and due to its resistance to acidic electrolyte, we choose glass as the most appropriate encapsulation material for PEC modules.

**Table S2.** Properties of six potential encapsulation materials for PEC modules.

| Material | Density | Elastic modulus | Specific embodied energy of 2 mm thick sheet |
|---|---|---|---|
| | *g/cm$^3$* | *Gpa* | *MJ/m$^2$* |
| Float glass | 2.5 | ~70 | 65 |
| Rigid PVC | 1.4 | ~3 | 170 |
| Polycarbonate | 1.2 | ~2.2 | 260 |
| Poly(methyl methacrylate) | 1.2 | ~2.6 | 340 |
| Aluminum | 2.7 | ~70 | 1050 |
| Stainless Steel | 7.9 | ~180 | 1230 |

The elastic modulus is a useful indicator of stiffness, although the overall "strength" of glass depends on several properties and cannot be expressed as a single number. It can, however, be characterized. For instance, Veer[S4] performed a set of experimental 3- and 4-point bending tests, with high numbers of repetitions on different thicknesses of glass, and generally found that glass fails at ~50-70 MPa for 2 mm thick plates (area dimensions 400x40 mm), but thicker plates—up to 8 mm—failed at roughly the same pressure. It is therefore clear that thickness alone does not determine resistance to breakage; surface defects are just as, if not more, important. Tempered, annealed and heat-treated glasses have reduced numbers of defects, thus increasing strength.

Standards exist for the types of glasses used in windows and other structural applications, generally referred to as "architectural" glass. These standards are based primarily on two performance characteristics: the maximum three-second wind gust and the maximum hailstone impact energy, and are both driven by glass thickness and, to a lesser extent, the type of heat treatment.

According to maps of US three-second maximum gust wind speeds (e.g.[S5]), ≥90 mph winds only occur near shorelines on the Gulf of Mexico and southern Atlantic Ocean, areas that are prone to hurricanes. For all other areas in the US, the maximum three-second gust wind speed is <90 mph. This corresponds to a design pressure (DP) rating of DP-20.[S6]

Cardinal Glass[S7,S8] provides thickness guides for glass usage. The lowest rating provided is DP-30, which recommends 2.2 mm thickness for heat-treated glass with 15 $ft^2$ (~1.4 $m^2$) spanned area and maximum length of 6 ft. (~1.8 m); for 20 $ft^2$ (~1.9 $m^2$), the recommended thickness is 3 mm. Annealed glass has somewhat more conservative requirements. The DP-20 ratings may be more lenient; however, we have assumed the DP-30 requirements for our analysis, limiting module sizes to ≤1.4 $m^2$ and ≤1.8 m on its longest side for 2 mm thickness. Furthermore, considering that our module uses two panes of glass rigidly connected by the PVC supporting ribs, we could then consider the total thickness instead of the individual pane thickness. In this case, 4 mm total thickness has a maximum span area of 30 $ft^2$ = 2.8 $m^2$ for heat-treated glass, which is more than adequate for our module size.

While the average glass thickness used by the PV industry ranges from ~2 to 6 mm,[S9] recent advances in process optimization have allowed some companies (e.g.[S10]) to reduce their maximum thicknesses from a "typical" 3 mm thickness for solar PV modules[S11] to 2.3-2.6 mm.

For hail, SolarWorld[S12] reports an impact test that "replicates a natural hail storm by dropping a 1.1-pound, one-inch steel ball onto solar panels from a height of 13 feet." This translates to an impact energy of 14.3 ft-lbs. (~19 J), equivalent to FM Class I-SH test hailstone of 45 mm (~1.75 inch) diameter. This is similar to testing for roofing materials.[S13] According to a US hail damage report,[S14] hail events are concentrated in the Great Plains region of the country, with a 50% risk of 1-inch (2.54 cm) or larger hailstones occurring at least once in five years. Probability drops off quickly outside this region. In areas where we expect most PEC systems to be located, e.g. high-insolation regions in the US desert southwest, the probability of large hail storms is extremely remote. A separate map of average hailstone diameter is similarly concentrated in the Great Plains, where it exceeds one inch (2.54 cm). In Arizona and New Mexico, the average diameter follows a strong gradient, ranging from <0.2 inch (<0.51 cm) in the west to 1.0 inch (2.54 cm) at the extreme eastern edge. This band of low-diameter hail extends upward into California and Nevada as well.

## S4. Module frame design

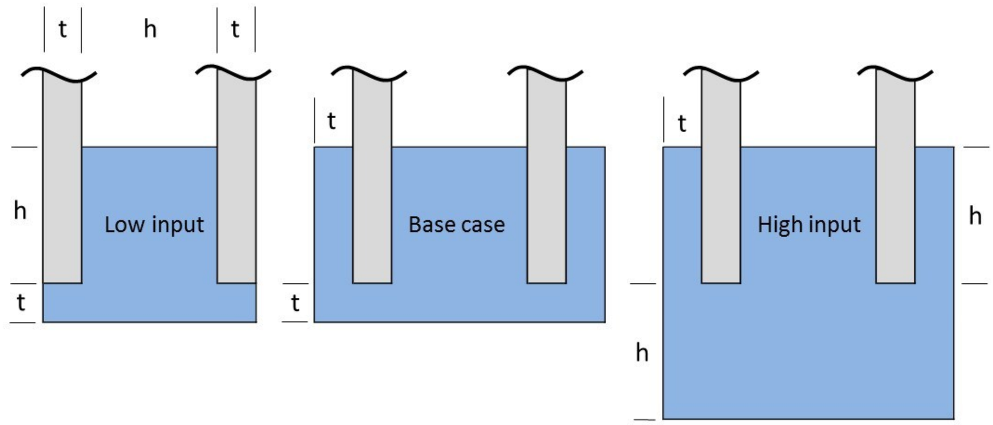


**Figure S3.** Dimensions of three alternative designs of PEC module frame, each made of PVC. The dimension “t” is the thickness of the glass window and back cover, and “h” is the inside dimension of the module enclosure.

## S5. Panel structural design

We perform an initial structural design of the panels, based on calculations of deflection under load. Considering the panel as a uniformly-loaded beam that is simply supported at three points (Figure S4, left), symmetry implies that deflection will be equal to a beam fixed on one end and simply supported on the other (Figure S4, right).

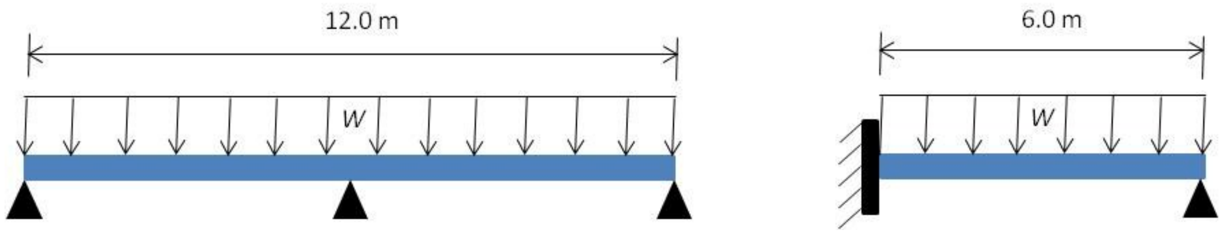


**Figure S4.** Estimation of panel deflection under load.

Based on Pope[S15], maximum deflection (inches) for a beam fixed on one end and simply supported on the other will be:

$$y_{max} = \frac{-0.0054\, W\, L^4}{E\, I}$$

where W is the uniform load (pounds inch$^{-1}$), L is the length of the beam (inch), E is the modulus of elasticity of the material (psi), and I is the moment of inertia of the beam (inch$^4$). In this deflection analysis we assume the panel is lying flat; the uniform load is composed of the dead load of the steel structure (1.0 pounds inch$^{-1}$) plus the load of the PEC components and electrolyte (2.2 pounds inch$^{-1}$), to which is applied a safety factor multiplier of 3. The length of the (half) panel is 6.0 m or 237 inches. The modulus of elasticity of steel is about $3.1 \times 10^7$ psi. A cross section of the panel structural frame member is shown in Figure S5. The moment of inertia of this section is 2.43 inch$^4$; this quantity is then doubled because the perimeter frame has two members. These properties yield a maximum calculated deflection of about 1.0 inch. The calculated length-to-deflection ratio is about 220, which is marginally acceptable for typical structural applications.

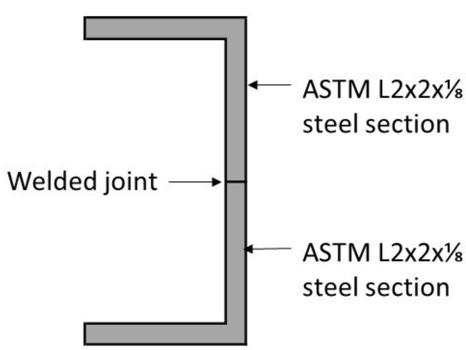


**Figure S5.** Cross section of panel perimeter structural frame.

The panel perimeter structural frame (Figure S5) is composed of 2 separate structural steel sections welded together, thus providing the same structural integrity with less material use compared to our earlier solutions employing a single larger steel section (Sathre et al. 2014). Although an improvement, this solution continues the use of "off the shelf" components for panel manufacture, which is appropriate for small-scale implementation of the technology. If PEC water splitting technology is to scale up as modeled in this analysis (employing almost 1.6 million individual panels per 1 GW facility), a much more rigorous structural optimization process is likely to be conducted, resulting in a more efficient structural solution using less steel material. Such optimization is analogous to the transition from traditional "body-on-frame" designs used previously by the automobile industry, to the more efficient "unibody" designs now used overwhelmingly in vehicles. MacKenzie et al.[S16] report that the switch to unibody car design has resulted in a weight reduction of 18.5% on average. We expect there is still scope for further panel material reductions if similar structural optimization process is employed for large-scale PEC panel manufacture.

## S6. Facility location and solar insolation

In our main analysis we consider the average solar insolation at four sites in the southwest US: Phoenix, Daggett, Tucson, and Las Vegas. Solar resource data are the average of monthly mean insolation on flat panels oriented south and tilted at the angle of latitude. In a sensitivity analysis, we also consider insolation data from a more representative selection of US sites: Charlotte, Omaha, Salt Lake City and Chicago. Details on solar insolation at each site are shown in Figure S6.

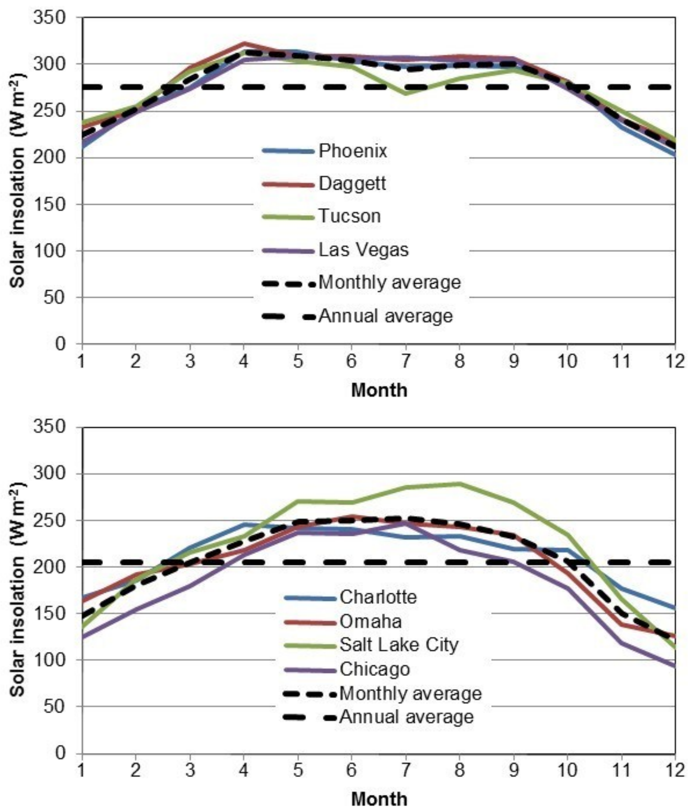


**Figure S6.** Solar insolation data for four US southwest locations used in our base-case analysis (top), and for four US north-central locations used in a sensitivity analysis (bottom).

## S7. Monte Carlo simulation of balance-of-system energy use

The balance of system (BOS) is characterized by a series of parameters describing aspects of panels, piping, gas handling, gas storage, water supply, roads, and facility operations. Each parameter is defined by a base-case value, a high energy input value, and a low energy input value (see Table S3).

**Table S3.** Parameter values describing the balance of system (BOS)

| Parameter description | Units | High input | Base case | Low input |
|---|---|---|---|---|
| **Panel** | | | | |
| Panel inactive area | percent | 15% | 10% | 5% |
| Panel material use | multiplier | 1.2 | 1.0 | 0.8 |
| Panel material energy intensity | multiplier | 1.2 | 1.0 | 0.8 |
| Panel internal frame spacing | meter | 0.5 | 1.0 | 1.5 |
| Panel transport (truck and train) | kilometer | 1300 | 300 | 0 |
| Containment vessel thickness | meter | 0.008 | 0.004 | 0.002 |
| Containment vessel material energy | multiplier | 1.5 | 1.0 | 0.8 |
| **Piping** | | | | |
| Maximum velocity, uncompressed $H_2$ | m $sec^{-1}$ | 0.5 | 1.0 | 2.0 |
| Maximum velocity, compressed $H_2$ | m $sec^{-1}$ | 20 | 40 | 60 |
| Maximum velocity, $H_2O$ | m $sec^{-1}$ | 1.0 | 3.0 | 5.0 |
| Material energy intensity | multiplier | 1.2 | 1.0 | 0.8 |
| Allowance for valves and fittings | percent | 50% | 25% | 10% |
| Pipe transport (train) | kilometer | 3000 | 1000 | 300 |
| **Gas handling** | | | | |
| Panels per blower | units | 50 | 100 | 150 |
| Gas blower power | kW | 3.0 | 1.5 | 0.7 |
| Gas blower average use | percent of capacity | 100% | 75% | 50% |
| Gas dryer power | kW | 5.0 | 2.4 | 1.4 |
| Gas dryer average use | percent of capacity | 100% | 75% | 50% |
| Compressor specific energy use | W h $m^{-3}$ | 82 | 70 | 57 |
| Compressor interstage loss | psi | 10 | 5 | 0 |
| Gas intake temperature | degree C | 80 | 60 | 40 |
| Compressor fan load | percent | 10% | 7.5% | 5% |
| Gas handling hardware embodied energy | multiplier | 2.0 | 1.0 | 0.5 |
| **Storage** | | | | |
| Gas storage capacity | day | 2.0 | 1.0 | 0.5 |
| Allowable stress in tank wall | multiplier | 0.8 | 1.0 | 1.2 |
| Corrosion allowance | mm | 12 | 9 | 6 |
| Allowance for valves and fittings | percent | 20% | 10% | 5% |
| **Water** | | | | |
| Water treatment electricity | MJ $ton^{-1}$ of treated water | 43.1 | 21.5 | 16.1 |
| Water treatment brine waste | liter $ton^{-1}$ of treated water | 774 | 387 | 71 |
| Water use for panel cleaning | liter $m^{-2}$ $year^{-1}$ | 100 | 25 | 10 |
| Water transport electricity | kWh $m^{-3}$ $km^{-1}$ | 0.0073 | 0.0047 | 0.0018 |
| **Roads** | | | | |
| Road width | meter | 8 | 6 | 4 |
| Asphalt thickness | meter | 0.10 | 0.05 | 0.03 |
| Subbase thickness | meter | 0.30 | 0.15 | 0.08 |
| Percent bitumen in asphalt | percent | 6% | 5% | 4% |
| Material energy intensity | multiplier | 1.2 | 1.0 | 0.8 |
| **Operations** | | | | |
| Number of trucks and cranes | units | 12 | 6 | 3 |
| Horsepower of engines | brake hp | 600 | 400 | 200 |
| Daily operating time | hours | 24 | 12 | 8 |

| | | | | |
|---|---|---|---|---|
| Equipment load factor | ratio | 0.70 | 0.54 | 0.38 |
| Panel heat requirement | kWh m$^{-2}$ year$^{-1}$ | 11.1 | 5.4 | 0.5 |

We use Monte Carlo simulations to estimate uncertainty introduced by interactions between multiple individual parameters describing the BOS. Simulation was conducted using Oracle® Crystal Ball software. Triangular probability distributions were assumed for each parameter based on low input, base-case and high input values (Table S3). A triangular distribution is defined by three points: the minimum, most likely, and maximum values. The high and low parameter values used in our study are selected as likely absolute minimums and maximums, and are thus well suited to a triangular distribution. Based on the outcome distribution of 10,000 simulations with simultaneous variation of each variable, the mean values of initial and continuing BOS energy inputs are used as base-case parameter values, and 90% confidence intervals are used as high input and low input parameter values. Because the BOS requirements of a fixed-output facility will depend on STH efficiency and cell life span, we conducted nine separate simulations considering each combination of these parameters. Outcomes are shown in Figure S6.

**Figure S7.** Outcomes of Monte Carlo simulations of BOS energy use, for nine combinations of STH efficiency and cell life span.

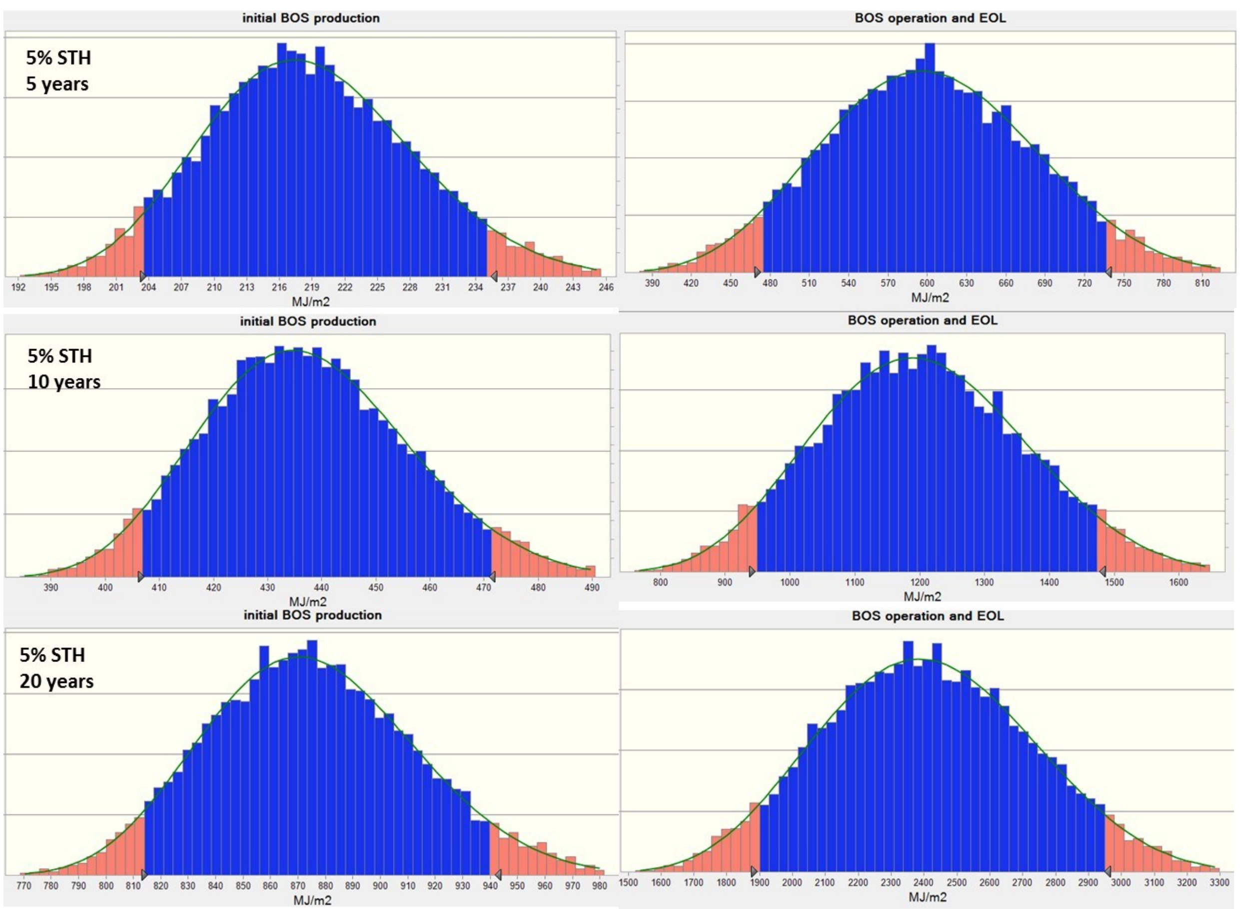

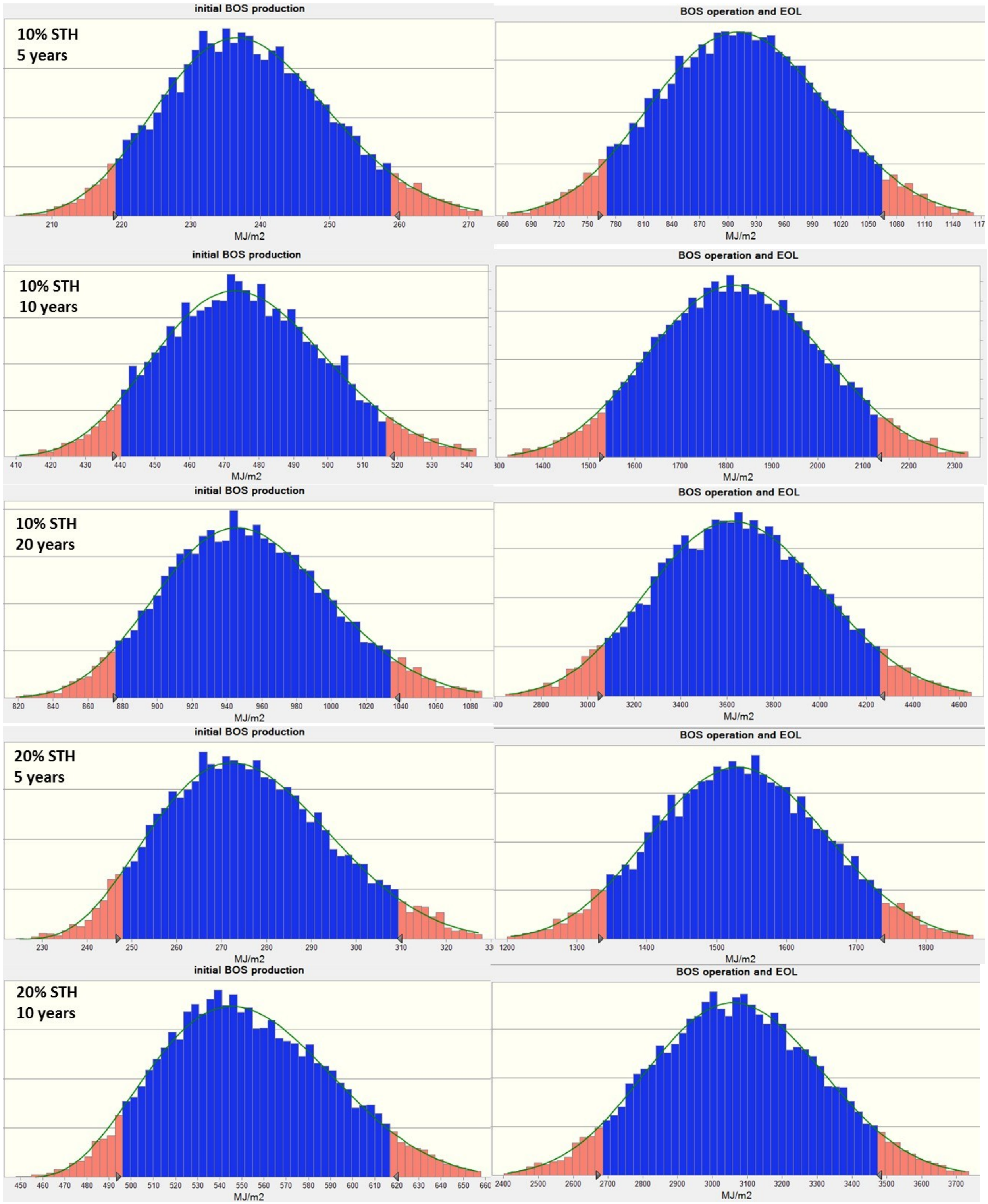
initial BOS production
BOS operation and EOL
10% STH
5 years
MJ/m2
initial BOS production
BOS operation and EOL
10% STH
10 years
MJ/m2
initial BOS production
BOS operation and EOL
10% STH
20 years
MJ/m2
initial BOS production
BOS operation and EOL
20% STH
5 years
MJ/m2
initial BOS production
BOS operation and EOL
20% STH
10 years
MJ/m2

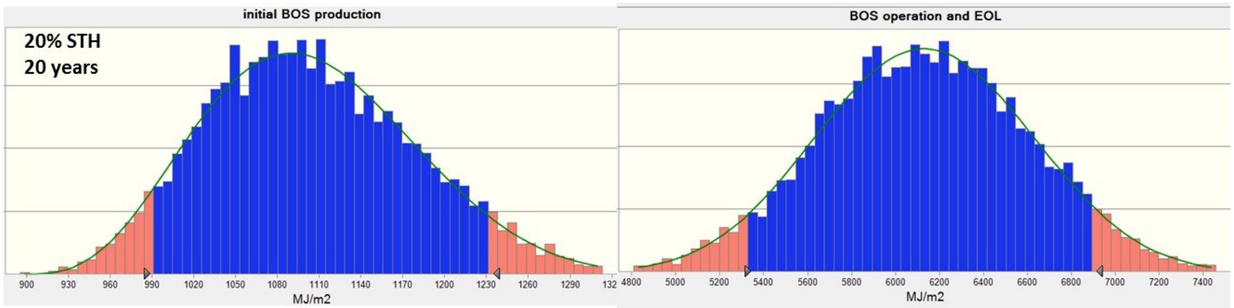
initial BOS production
20% STH
20 years
900
930
960
990
1020
1050
1080
1110
1140
1170
1200
1230
1260
1290
132
MJ/m2
BOS operation and EOL
4800
5000
5200
5400
5600
5800
6000
6200
6400
6600
6800
7000
7200
7400
MJ/m2

## S8. Module heating to avoid freezing

Per the analysis described by Sathre et al.[S17], heating of modules may be required to prevent freezing of the electrolyte during cold weather. The freezing temperature of 1 molar sulfuric acid is approximately -5 °C. If the PEC cells drop below this temperature, they will freeze, potentially rupture, and fail. To prevent freezing, the underside of each module could be fitted with an electrically powered strip heater to provide heating when the embedded temperature sensors determine this necessary. This heater can also be backed by a layer of insulation. We used a computational model to assess the degree of heating required for the modules, to estimate its effect on the facility's net energy production. Given the small aspect ratio of the modules (thickness divided by length or width), a one-dimension finite-difference transient heat transfer model was constructed, with coupled heat transfer equations solved for each hour of the year for the top window, anolyte, light absorber assembly, catholyte, case backing, strip heater and (when applicable) insulation layers. It was assumed that the modules only transfer heat out to the environment via radiation and convection. These modules would heat up in the daytime due to the conversion of insolation into waste heat in the light absorber assembly and in the semitransparent top window; joule heating of the electrolyte was ignored given the low current densities of this device. If the temperature of the device dropped below a temperature threshold of -2.5 °C, a one-dimension steady-state heat transfer model was used to estimate the required heater energy input to prevent the electrolyte temperature from dropping further. This minimum temperature threshold is greater than the electrolyte freezing temperature to provide an operational safety margin.

In our earlier analysis[S17], we estimated the total annual electricity requirement for heating. This varied between the four selected sites in the US southwest, with Daggett requiring the most at 11.0 kWh $m^{-2}$ $yr^{-1}$, and Phoenix needing the least at 0.6 kWh $m^{-2}$ $yr^{-1}$. The average of the sites is 5.4 kWh $m^{-2}$ $yr^{-1}$, which we adopt as our base-case heating requirement. Although the internal convection coefficients of the louvered design are different from the previous micro-wire system, resultant from the changes to the internal cell geometry, we assume this will not change the heating energy needs.

## S9. Hydrogen demand scale-up scenarios

We conduct a scale-up analysis to estimate required quantities of thin film materials and identify potential constraints in material availability. We consider three hydrogen demand scale-up scenarios of varying extent: Use of hydrogen fuel in 10% of the US passenger car and light truck fleet would require 14 facilities producing 1 GW (continuous annual average) each. Use of hydrogen fuel in 100% of the US light vehicle fleet through 2040 would require 142 1 GW facilities. Global scale-up through 2040 to cover the demand of all light duty vehicles is projected to require 850 facilities of 1 GW each.

US light-duty vehicle travel demand in 2040 is estimated to be 3.57 trillion miles.[S18] Based on NAS[S19], we assume that by 2040 average light-duty vehicle hydrogen fuel cell efficiency will be 8.8 kg $H_2$ per 1000 miles (based on the average of passenger car and light truck efficiencies), roughly five times more efficient than current conventional gasoline engines. This results in an annual demand of 31.4 billion kg $H_2$ in 2040. Since each 1 GW facility produces 222 million kg $H_2$ per year, about 142 such facilities would be required to fully meet US demand. If 10% of US vehicles were hydrogen-powered, about 14 facilities would be required. Extrapolating globally, demand for petroleum for transportation in 2040 is projected to be roughly six times that in the US. Assuming this applies to light-duty vehicle demand, and that all vehicles are hydrogen-powered in 2040, approximately 850 1 GW plants would be required globally.

The total PEC cell area required is based on 10% STH efficiency, with annual material requirements based on a 10-year cell life span. Our calculations use our base-case value of 50% material utilization efficiency in thin film deposition, which assumes that half of the material is deposited on the substrate and the other half is wasted (material utilization efficiency is discussed in Section 2.2.1). Waste recovery efforts would likely be employed for high value materials, thus we likely overestimate the consumption of such materials. Results are summarized in Figure S7, and detailed in Table S4.

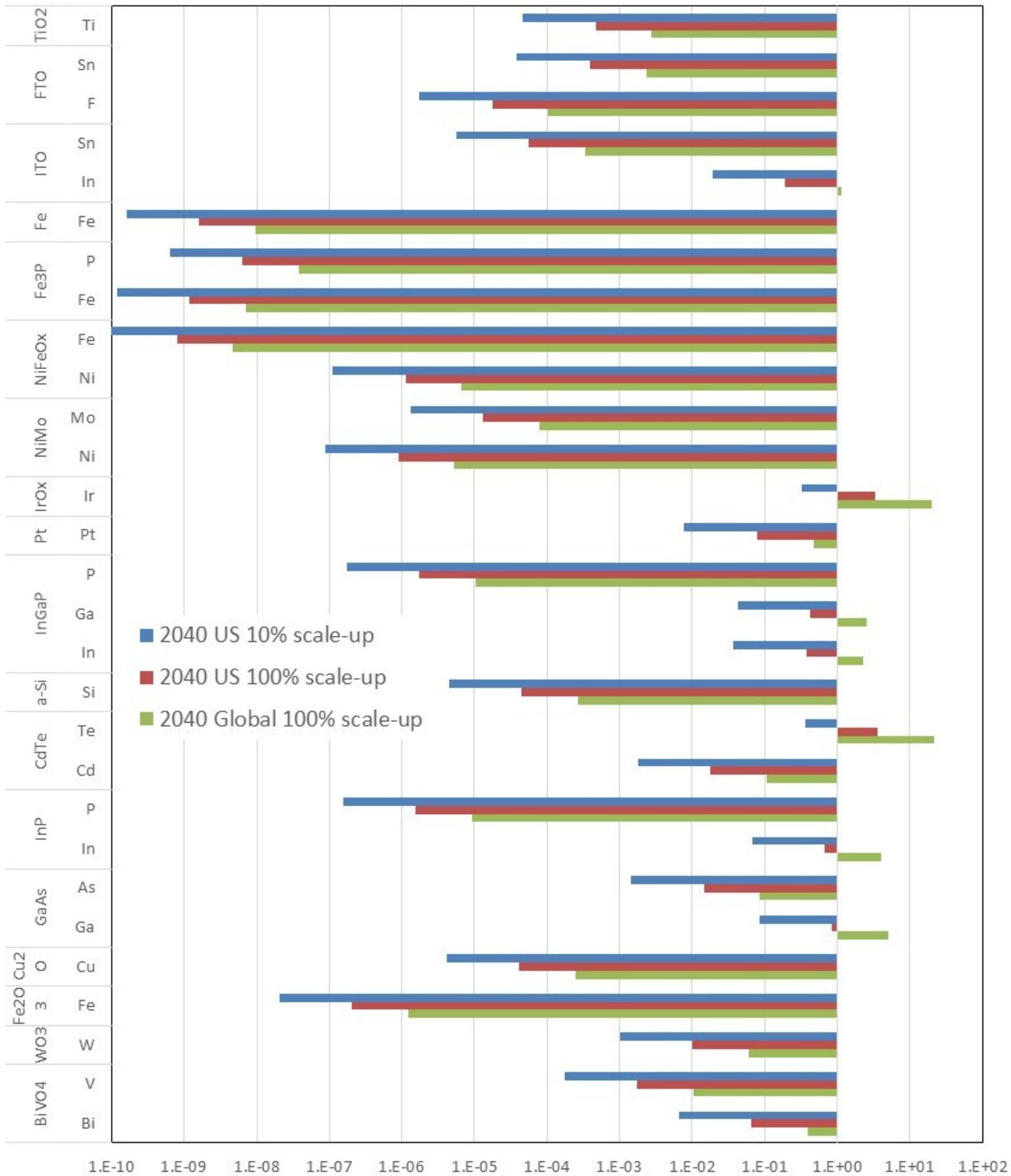


**Figure S8.** Amount of thin film materials needed for PEC hydrogen production at 3 scale-up levels, expressed as proportion of 2014 global primary production (i.e., 1 is 100% of 2014 production, 0.1 is 10% of 2014 production, etc.).

**Table S4.** Amount of thin film materials needed for PEC hydrogen production, expressed as tons of materials contained in an operating 1GW facility, tons of materials needed annually for three scale-up levels, and percentage of 2014 global primary production for three scale-up levels.

| | | | Tons per year needed | | | Percent of 2014 mine production | | |
|---|---|---|---|---|---|---|---|---|
| Thin film material | Element | Tons per facility | 2040 US 10% scale-up | 2040 US 100% scale-up | 2040 Global 100% scale-up | 2040 US 10% scale-up | 2040 US 100% scale-up | 2040 Global 100% scale-up |
| *Photoelectrode layers (250 nm)* | | | | | | | | |
| $BiVO_4$ | Bi | 39.4 | 56 | 560 | 3351 | 0.66% | 6.6% | 39% |
| | V | 9.6 | 14 | 136 | 817 | 0.02% | 0.17% | 1.0% |
| $WO_3$ | W | 58.6 | 83 | 832 | 4982 | 0.10% | 1.0% | 6.0% |
| $Fe_2O_3$ | Fe | 41.5 | 59 | 589 | 3526 | <0.001% | <0.001% | <0.001% |
| $Cu_2O$ | Cu | 55.0 | 78 | 781 | 4676 | <0.001% | 0.004% | 0.025% |
| GaAs | Ga | 26.5 | 38 | 376 | 2250 | 8.5% | 85% | 510% |
| | As | 28.4 | 40 | 404 | 2418 | 0.14% | 1.4% | 8.6% |
| InP | In | 39.1 | 56 | 555 | 3324 | 6.8% | 68% | 400% |
| | P | 10.5 | 15 | 150 | 897 | <0.001% | <0.001% | 0.001% |
| CdTe | Cd | 28.3 | 40 | 402 | 2404 | 0.18% | 1.8% | 11% |
| | Te | 32.1 | 46 | 456 | 2729 | 36% | 370% | 2200% |
| a-Si | Si | 24.1 | 34 | 342 | 2045 | <0.001% | 0.004% | 0.027% |
| InGaP | In | 21.5 | 31 | 306 | 1829 | 3.7% | 37% | 220% |
| | Ga | 13.1 | 19 | 186 | 1111 | 4.2% | 42% | 250% |
| | P | 11.6 | 16 | 165 | 987 | <0.001% | <0.001% | 0.001% |
| *Catalyst layers (1 nm)* | | | | | | | | |
| Pt | Pt | 0.89 | 1.3 | 13 | 75 | 0.78% | 7.8% | 47% |
| IrOx | Ir | 0.93 | 1.3 | 13 | 79 | 33% | 330% | 1970% |
| NiMo | Ni | 0.15 | 0.2 | 2.1 | 13 | <0.001% | <0.001% | 0.001% |
| | Mo | 0.25 | 0.35 | 3.5 | 21 | <0.001% | 0.001% | 0.008% |
| NiFeOx | Ni | 0.19 | 0.27 | 2.7 | 16 | <0.001% | <0.001% | 0.001% |
| | Fe | 0.16 | 0.23 | 2.3 | 13 | <0.001% | <0.001% | <0.001% |
| $Fe_3P$ | Fe | 0.23 | 0.33 | 3.3 | 20 | <0.001% | <0.001% | <0.001% |
| | P | 0.04 | 0.062 | 0.6 | 3.7 | <0.001% | <0.001% | <0.001% |
| Fe | Fe | 0.32 | 0.46 | 4.6 | 28 | <0.001% | <0.001% | <0.001% |
| *Other layers* | | | | | | | | |
| ITO (200 nm) | In | 11.0 | 16 | 156 | 933 | 1.9% | 19% | 114% |
| | Sn | 1.2 | 1.6 | 16 | 99 | <0.001% | 0.006% | 0.033% |
| FTO (200 nm) | F | 4.1 | 6 | 58 | 348 | <0.001% | 0.002% | 0.010% |
| | Sn | 8.1 | 11 | 115 | 686 | 0.004% | 0.039% | 0.23% |
| $TiO_2$ (60 nm) | Ti | 6.3 | 9 | 89 | 534 | 0.005% | 0.047% | 0.28% |

**S10. Additional references used in the Supplementary Information**

S1 ETH Zurich, *The Finechem Tool*, 2010. http://www.sust-chem.ethz.ch/tools/finechem.

S2 G. Wernet, S. Papadokonstantakis, S. Hellweg and K. Hungerbuhler, Bridging data gaps in environmental assessments: Modeling impacts of fine and basic chemical production, *Green Chem*., 2009, 11, 1826–1831.

S3 R. Sathre and E. Masanet, Long-term energy and climate implications of carbon capture and storage deployment strategies in the US coal-fired electricity fleet. *Environmental Science & Technology*, 2012, **46**, 9768–9776.

S4 F.A. Veer, The strength of glass, a nontransparent value, *Heron Journal*, 2007. http://heronjournal.nl/52-12/4.pdf

S5 WindSpeedByZip, *Wind Speed By Zip*, 2015. http://www.windspeedbyzip.com/

S6 National Certified Testing Laboratories, *Wind Velocity Chart*, 2015. http://www.nctlinc.com/velocity-chart/

S7 Cardinal IG Company, *Glass Windload Tables*, Technical service bulletin #IG03, 2008. http://www.cardinalcorp.com/wp-content/uploads/pdf/tsb/ig/IG03_05-08.pdf;

S8 Cardinal IG Company, *Technical Glass Guide, Version 2.0*, 2014. http://www.cardinalcorp.com/wp-content/uploads/pdf/Technical_Glass_Guide_Web.pdf

S9 PPG, *Solarphire™ PV High-Transmissive Glass*, 2010. http://www.ppg.com/en/solutionbyindustry/energy/solar/documents/finalsolarphirepvproductdatasheet.pdf

S10 PV Tech, *Centrosolar Glas offers 30% reduction of module glass thickness and weight*, 2012. http://www.pv-tech.org/product_reviews/centrosolar_glas_offers_30_reduction_of_module_glass_thickness_and_weight

S11 Green Rhino Energy, *Solar Glass & Mirrors* , 2013. http://www.greenrhinoenergy.com/solar/technologies/solar_glass.php

S12 SolarWorld Americas, *The SolarWorld Standard* , 2015. http://www.solarworld-usa.com/why-choose-solarworld/the-solarworld-standard

S13 V. Crenshaw and J.D. Koontz, *Simulated Hail Damage and Impact Resistance Test Procedures for Roof Coverings and Membranes*, 2000. http://jdkoontz.com/articles/simulated.pdf

S14 S.A. Chagnon, D. Chagnon and S.D. Hilbert, *Hailstorms across the Nation: An Atlas about Hail and Its Damages*, Illinois State Water Survey, Contract Report 2009-12, 2009. http://www.isws.illinois.edu/pubdoc/CR/ISWSCR2009-12.pdf

S15 J.E. Pope, *Rules of Thumb for Mechanical Engineers*, Gulf Publishing Company, Houston, 1997.

S16 D. MacKenzie, S. Zoepf and J. Heywood, Determinants of US passenger car weight, *Int. J. of Vehicle Design*, 2014, **65**, 73-93.

S17 R. Sathre, C.D. Scown, W.R. Morrow, J.C. Stevens, I.D. Sharp, J.W. Ager, K. Walczak, F.A. Houle and J.B. Greenblatt, Life-cycle net energy assessment of large-scale hydrogen production via photoelectrochemical water splitting, *Energy Environ. Sci*., 2014, **7**: 3264-3278.

S18 Energy Information Administration (EIA), *Annual Energy Outlook 2015*, US Department of Energy, 2015. http://www.eia.gov/forecasts/aeo/.

S19 National Academies of Science (NAS), *Transitions to Alternative Vehicles and Fuels*, The National Academies Press, Washington DC, 2013. http://www.nap.edu/catalog.php?record_id=18264.